Radio Science

RESEARCH ARTICLE
10.1029/2018RS006589

Special Section:
URSI General Assembly and Scientific Symposium (2017)

Polar Topside Ionosphere During Geomagnetic Storms: Comparison of ISIS-II With TDIM

J. J. Sojka[1,2], D. Rice[2], V. Eccles[2], M. David[1], R. W. Schunk[1], R. F. Benson[3], and H. G. James[4]

[1]Center for Atmospheric and Space Sciences, Utah State University, Logan, UT, USA, [2]Space Environment Corporation, Logan, UT, USA, [3]Geospace Physics Laboratory, Heliophysics Science Division, NASA Goddard Space Flight Center, Greenbelt, MD, USA, [4]Natural Resources Canada Geomagnetic Laboratory, Ottawa, Ontario, Canada

Key Points:
- The paper focuses on prestorm and main phase topside ionospheric response to a mild and a severe geomagnetic storm
- Simulations from an extensively used *F* region model, TDIM, are compared to ISIS-II topside ionosphere observations
- Surprisingly, the TDIM is unable to simulate the observed storm response while satisfactorily simulating the prestorm topside

Correspondence to:
J. J. Sojka,
jan.sojka@usu.edu

Citation:
Sojka, J. J., Rice, D., Eccles, V., David, M., Schunk, R. W., Benson, R. F., & James, H. G. (2018). Polar topside ionosphere during geomagnetic storms: Comparison of ISIS-II with TDIM. *Radio Science*, *53*, 906–920. https://doi.org/10.1029/2018RS006589

Received 23 MAR 2018
Accepted 14 JUN 2018
Accepted article online 23 JUN 2018
Published online 14 JUL 2018

Abstract Space weather deposits energy into the high polar latitudes, primarily via Joule heating that is associated with the Poynting flux electromagnetic energy flow between the magnetosphere and ionosphere. One way to observe this energy flow is to look at the ionospheric electron density profile (EDP), especially that of the topside. The altitude location of the ionospheric peak provides additional information on the net field-aligned vertical transport at high latitudes. To date, there have been few studies in which physics-based ionospheric model storm simulations have been compared with topside EDPs. A rich database of high-latitude topside ionograms obtained from polar orbiting satellites of the International Satellites for Ionospheric Studies (ISIS) program exists but has not been utilized in comparisons with physics-based models. Of specific importance is that the Alouette/ISIS topside EDPs spanned the timeframe from 1962 to 1983, a period that experienced very large geomagnetic storms. We use a physics-based ionospheric model, the Utah State University Time Dependent Ionospheric Model (TDIM), to simulate ionospheric EDPs for quiet and storm high-latitude passes of ISIS-II for two geomagnetic storms. This initial study finds that under quiet conditions there is good agreement between model and observations. During disturbed conditions, however, a large difference is seen between model and observations. The model limitation is probably associated with the inability of its topside boundary to replicate strong outflow conditions. As a result, modeling of the ionospheric outflows needs to be extended well into the magnetosphere, thereby moving the upper boundary much higher and requiring the use of polar wind models.

1. Introduction

At high latitudes, the topside ionosphere responds to a variety of magnetospheric, ionospheric, and thermospheric processes. For example, the magnetospheric convection electric field leads to Joule heating and enhanced transport that includes vertical raising/lowering of the topside ionosphere. In addition, auroral and polar cap precipitation of both electrons and protons leads to enhanced densities of the topside, while an energy deposition into the thermosphere leads to modifications to the topside neutral composition, temperature, and winds that modify the topside ionosphere. The ion and electron temperatures respond to all these processes and, in turn, dramatically control the topside scale height as well as the polar wind outflows into the magnetosphere. Under extreme geomagnetic conditions, the topside ionosphere is not in diffusive equilibrium. All these processes combine, and evidence of them can be found in the topside electron density profile (EDP). Present-day modeling of the ionosphere, coupled ionosphere-thermosphere, coupled ionosphere-magnetosphere, and the fully coupled thermosphere-ionosphere-magnetosphere include many of these processes. However, the calibration/validation of these kinds of model storm simulations of the topside is still in its infancy in comparison to calibration using observed N_mF_2, h_mF_2, and total electron content or in situ measurements of Te and Ti.

The special issue of the monthly Proceedings of Institute of Electrical and Electronics Engineers (IEEE) in June 1969 provided an extensive overview of a technique for observing the topside ionosphere, the satellite-borne topside sounder (Institute of Electrical and Electronics Engineers, 1969). Chan and Colin (1969) reviewed and summarized the global electron density distributions from topside soundings, while Warren (1969) reviewed the topside ionospheric response to geomagnetic storms. A brief report by Norton (1969) in this particular issue of proceedings of IEEE proposed that in order to explain the midlatitude morning springtime topside

EDP depletion during a $Kp = 8$ geomagnetic storm, the O^+ loss rate must be increased by a factor of 16. In Norton's Figure 1, based on topside and ground-based soundings, he also showed how the EDP was modified during the storm. Sato and Colin (1969) carried out an extensive analysis of 1200 Alouette-1 topside sounder passes at high latitudes to establish the seasonal, local time, and geomagnetic activity morphologies. Their study was based on electron density values at the height of Alouette 1 (average height of 1,040 km). Sato and Chan (1969) considered 24 geomagnetic storms and focused on their impact on the high-latitude topside. They used the complete Alouette-1 topside EDPs. One specific finding was that under the most severe storms, the EDPs from the high-latitude and polar regions are reduced in density almost everywhere but that there were also regions with strong enhancements depending on magnetic local time, invariant latitude, and altitude. This result is consistent with that of Nishida (1967). Dayharsh and Farley (1965) separated electron density values at the height of Alouette 1 (1,000 km) into seasonal, diurnal, and magnetic activity groups and found storm-induced depletions at auroral latitudes and over a large range of L values on summer days. Reports on how the temperature, electrons, or ions responded to geomagnetic storms at high latitudes were somewhat mixed. Willmore (1965) and Titheridge and Andrews (1967) reported cooling, while Watt (1966) and Nishida (1967) reported heating.

In terms of magnetospheric-ionospheric coupling, especially the flow of heavy ions into the magnetosphere, Wahlund et al. (1992) used European incoherent scatter radar to study and define two types of large-scale bulk outflow. The study identified cases of outflow of O^+ that reached 2×10^{10} cm^{-2}/s. Their results quantified strong outflows observed by Lockwood and Titheridge (1981) who used Alouette-1 topside EDPs. Ogawa et al. (2003) used the Svalbard European scatter radar to correlate 170 outflow events with soft (<1 keV) precipitation. These corresponded to the type II events defined by Wahlund et al. (1992). Several authors also observed strong outflows associated with strong storm-enhanced density events in the cusp region, resulting in polar cap tongues of ionization (Foster et al., 2005; Yuan et al., 2008). The source of this outflow, the enhanced F region density of the storm-enhanced density, was described by Foster et al. (2005) as a third outflow mechanism. Zeng and Horwitz (2007, 2008) modeled this third mechanism using a dynamic fluid kinetic model. Recently, Zou et al. (2017) used the Poker Flat ISR and Defense Meteorological Satellite Program satellite in situ plasma measurements to study Type-II outflow events in the context of the global magnetohydrodynamic ionospheric-magnetospheric model on the Space Weather Modeling framework. The emphasis of this study, however, was the overall morphology and not the specific outflow or topside model validation.

Benson et al. (2016) motivated by a magnetospheric study of Osherovich et al. (2007) that showed electron density enhancements observed by the Imager for Magnetopause-to-Aurora Global Exploration satellite near its 8 R_E apogee with fluctuations that were correlated with solar wind variations and the work of Tu et al. (2007) that showed the enhancements extended down to 4 R_E extended this research to lower altitudes using high-latitude topside sounder data from the International Satellites for Ionospheric Studies (ISIS) program. Their results based on 10 major geomagnetic storms identified day/night differences in response as well as suggested correlations with solar wind parameters. They found that large EDP depletions exist in the Northern Hemisphere winter and spring daytime, while during Northern Hemisphere winter nighttime the EDP is enhanced during the storm. Kitamura et al. (2012, 2010) used the Akebono topside sounder to study the response of Ne at high altitudes to geomagnetic storms and observed large storm-induced magnetospheric enhancements.

Although extensive observational topside EDP data exist and extensive analysis has led to a wide range of findings, including some apparently contradictory conclusions, and the EDP have been used in empirical models (e.g., see Bilitza, 2009; Reinisch et al., 2007), there have been relatively few direct comparisons between simulations based on physics-based models and these topside EDP observations. We attempt to address this challenge by carrying out this study based on an initial pair of geomagnetic storms. In section 2, we introduce the ISIS-II topside EDPs, while section 3 describes the specific physics-based ionospheric model, the Time Dependent Ionospheric Model (TDIM). The limitations of these model comparisons are defined and examined by how the simulations compare with the observations in section 4. Section 5 compares our results with those of earlier studies. It also identifies a weakness in TDIM with respect to topside ionospheric modeling during magnetic storms. Our key results and future work are summarized in section 6.

2. Topside Ionosphere Observations

2.1. ISIS Topside Sounder Program

The ISIS was a joint Canadian-American program that included four Canadian satellites: Alouette-1, Alouette-2, ISIS-1, and ISIS-II. Each of these satellites, which were launched into polar orbits between 1962 and 1971, carried a topside sounder instrument. ISIS-II, the source of the topside ionograms used in this report, operated between 1971 and 1990 (Daniels, 1971). The technical issues involved in operating a topside sounder instrument are detailed in a special issue of the Proceedings of the IEEE, June 1969 (Vol 57, No. 6), and the scientific analysis of these ionograms is reviewed by Jackson et al. (1980) and Benson (2010).

The ISIS program was supported by more than 20 ground receiving stations. Ionograms from the four satellites were recorded on seven-track tape, and some were transcribed to 35-mm film. Over 177,000 of the millions of ionograms recorded were converted to EDPs (Benson and Bilitza, 2009). For this study, archived ionograms on 35-mm film from the Resolute Bay Canadian polar cap station (74.7°N, 265.1°E) were used. The recovery of Alouette/ISIS topside data from seven-track analog tapes and the subsequent ionogram conversion to EDPs is described by Benson (1996), Benson and Bilitza (2009), and Benson et al. (2012). This restoration and preservation project was initiated by the National Aeronautics and Space Administration (NASA) Ionospheric/thermospheric/mesospheric (ITM) Data Evaluation Panel, which also initiated a similar program to restore the 35-mm film archive (Rice et al., 2015, 2017) in 2014. These two restoration programs and the 177,000 EDPs were organized to avoid duplication. The primary data archive is the NASA Space Physics Data Facility accessed via the website http://spdf.gsfc.nasa.gov/isis/isis-status.html.

2.2. Film Recovery

In 2014, Space Environment Corporation (SEC) arranged for the loan of 34 reels of ISIS-II 35-mm film from the Canadian Communications Research Centre, Ottawa, Canada, archive. These film reels were commercially scanned at $40/reel. Each reel of film contained a dozen or more orbit passes over the receiving station. Each pass may have over 10 useful ionograms, depending on the instrument mode and the location of the pass with respect to the receiving station. Resolute Bay was the ground receiving station for these data. The scanned film was made with a pixel resolution corresponding to 0.5 km/pixel, which is well over the original scientific content on the film. The files comprised fixed length scans that had a 5% overlap with the next file. The process of scientific frame identification was not part of the commercial film scanning. SEC undertook the software development to carry out the following procedures:

1. Software capable of stitching the files together
2. Frame identification
3. Frame coordinate registration
4. Read ephemeris data from digitized film
5. Scale and invert ionograms traces to yield EDPs
6. Develop SEC scripts to archive both these extracted ionograms and their associated EDPs.

Under follow-on work, the full set of topside ionograms, digitized from the 34 reels, will be processed and made available to the research community at the NASA Space Physics Data Facility.

2.3. Two Storm Periods

A study focused on retrieving EDPs from two storm periods was undertaken. The two storms occurred on day 101, 11 April 1973 (STORM1) and day 170, 18 June 1972 (STORM2). Figure 1 shows the geomagnetic and solar conditions for STORM1 and STORM2 in the left and right columns, respectively. The top panel contrasts the ring current storm index Dst, showing that STORM1 reached −65 nT, while STORM2 almost reached −200 nT. This difference in ring current strength is also reflected in the contrast between the 3-hr planetary index Kp (middle panels), with STORM1 reaching a Kp of 5− and STORM2 reaching a maximum of 8+. The solar radio flux index F10.7 and the 81-day center average (F10.7A) changed by more than 30 units from STORM1 at $F10.7A = 102$ to STORM2 $F10.7A = 135$. For each storm, both a prestorm pass and a pass made during the storm were processed. Vertical dashed lines in the top four panels show the respective times of these orbits. The passes were chosen at universal times (UTs) such that they crossed over the polar region at similar latitudes and local times.

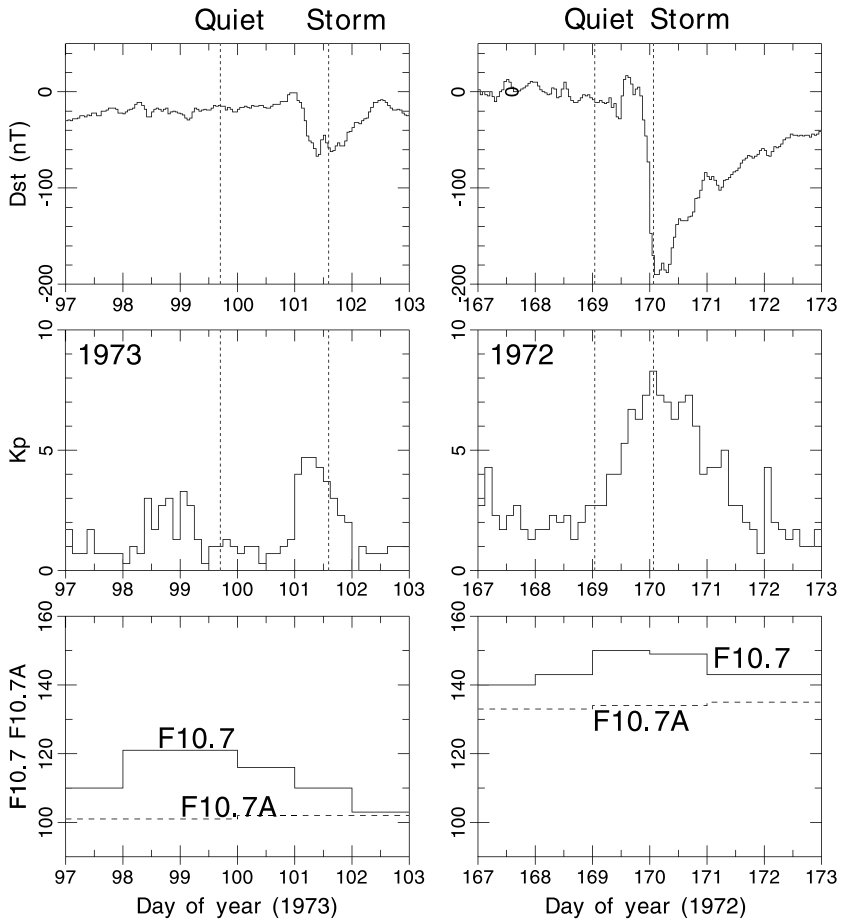

Figure 1. Geomagnetic indices Dst (top panel) and Kp (middle panel) together with solar radio flux indices F10.7 and F10.7A (lower panel) for the two storm periods of interest in this study. Vertical dashed lines in the top two rows identify the times of the International Satellites for Ionospheric Studies-II orbit segments used in this study.

2.3.1. STORM1

Both the prestorm and storm passes for which topside ISIS-II ionograms were processed are identified in Figure 2a. Symbols represent the satellite positions at 1-min intervals. The prestorm *quiet* pass began at 16:49 UT on day 99, 1973, while the storm pass began at 14:16 UT on day 101, 1973. Both passes are located at high latitudes poleward of 70°magnetic latitude. Using analysis described by Rice et al. (2015, 2017), the 11 quiet pass and 21 storm pass ionograms were inverted into topside EDPs. (The storm pass had twice as many ionograms due to the ISIS-II observation mode being changed.) Figure 2b shows the EDPs from the ISIS-II pass on day 99, 1973 (left panel) and the pass on day 101, 1973 (right panel). A number of differences in the EDPs exist between the two data sets. In the topside, above 500 km, the storm electron densities are systematically lower than those in the quiet pass. This difference is also true at the lowest heights though not as apparent. These differences in density are about 30%.

Another systematic difference between the two passes is the lowest altitude of the EDPs. For the quiet pass (left panel, Figure 2b), it lies between 200 and 280 km. In contrast, during the storm pass, particularly toward the end of the pass, the lowest altitudes are below 200 km. This difference in lowest altitude will become better defined in the STORM2 comparison. The location of this lower altitude provides key information about the relative roles of the F2, F1, and *E* region peak densities.

2.3.2. STORM2

The second storm occurred near midsummer conditions for the northern polar region, hence in strongly sunlit conditions. Figure 2c shows the location of ISIS-II at 1-min intervals for both the quiet (square symbols) and the storm (diamond symbols) pass. These two passes cross the central polar region from late evening local time to midmorning dayside local time. The start and end times of the passes are identified in Figure 2c.

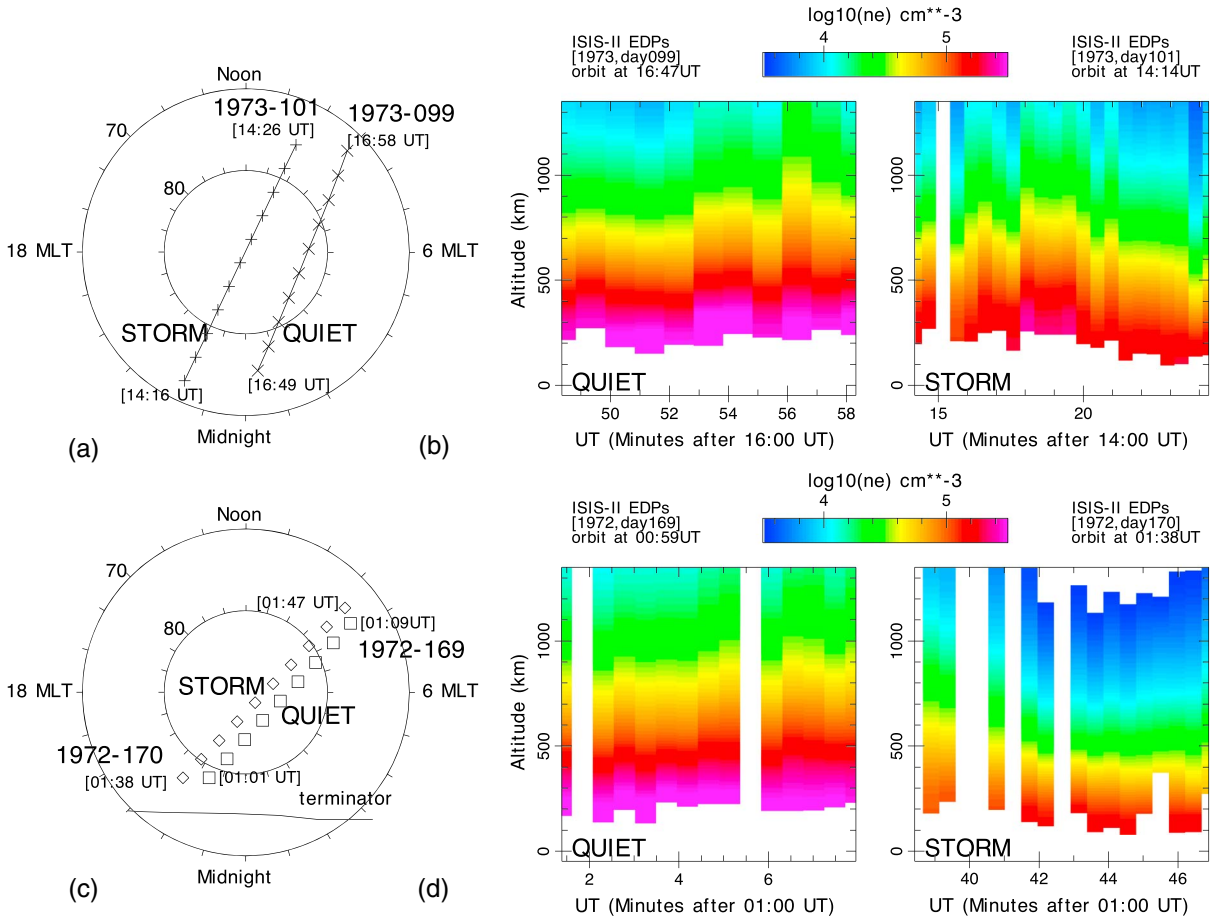

Figure 2. (a) ISIS-II satellite locations at 1-min intervals for two passes when data were downlinked to Resolute Bay, Canada. Each pass is plotted in a magnetic latitude-magnetic local time polar diagram. (b) Inferred EDPs from ISIS-II ionograms, taken on day 99, 1973 (left color panel) and on day 101, 1973 (right color panel). The EDP densities are color coded on a logarithmic scale. The solar terminator is identified and labeled. (c) ISIS-II satellite locations for two passes downlinked to Resolute Bay on days 169 and 170, 1972. (d) Inferred EDP from ISIS-II ionograms on day 169 and 170 (right color panel) 1972. ISIS = International Satellites for Ionospheric Studies; EDP = electron density profile; MLT = magnetic local time.

A total of 15 ionograms was obtained on the quiet pass, but of these, only 13 were suitable for conversion to EDPs. On the storm pass, 19 ionograms were obtained, but only 14 were suitable for conversion to EDPs. These EDPs are plotted in Figure 2d. The left panel shows the electron density for the quiet pass. A comparison between these two passes shows that the storm pass electron densities are extensively reduced at all altitudes by factors ranging from 2 to 4.

In the quiet pass, the lowest altitudes associated with the inversion of ionograms lie between 150 and 220 km. On the storm pass, the initial lowest altitudes are in the 200-km range but many of the later profiles, dayside solar conditions, have lower altitudes down to 100 km.

A comparison of STORM1 (Figure 2b) and STORM2 (Figure 2d) shows that the quiet passes are similar. However, the storm passes from a weak storm (Figure 2b, right panel) to a strong storm (Figure 2d, right panel) reveal a significant dependence on geomagnetic conditions given that the observation of the two events, their satellite locations, is somewhat similarly located relative to magnetospheric (auroral) and ionospheric (terminator) boundaries. The trends shown in electron density variation between quiet and storm passes are significant in all cases. Rice et al. (2015, 2017) provided information on how accurately the topside ionogram traces can be identified and subsequently inverted using two independent techniques. Their results indicate that the inversion procedure has uncertainty in densities less than 20%. However, in contrast, the uncertainty on lowest altitudes is large. During quiet periods, the expectation would be that the lowest altitudes would be slightly above the F2 layer peak. Prior studies comparing topside and bottomside

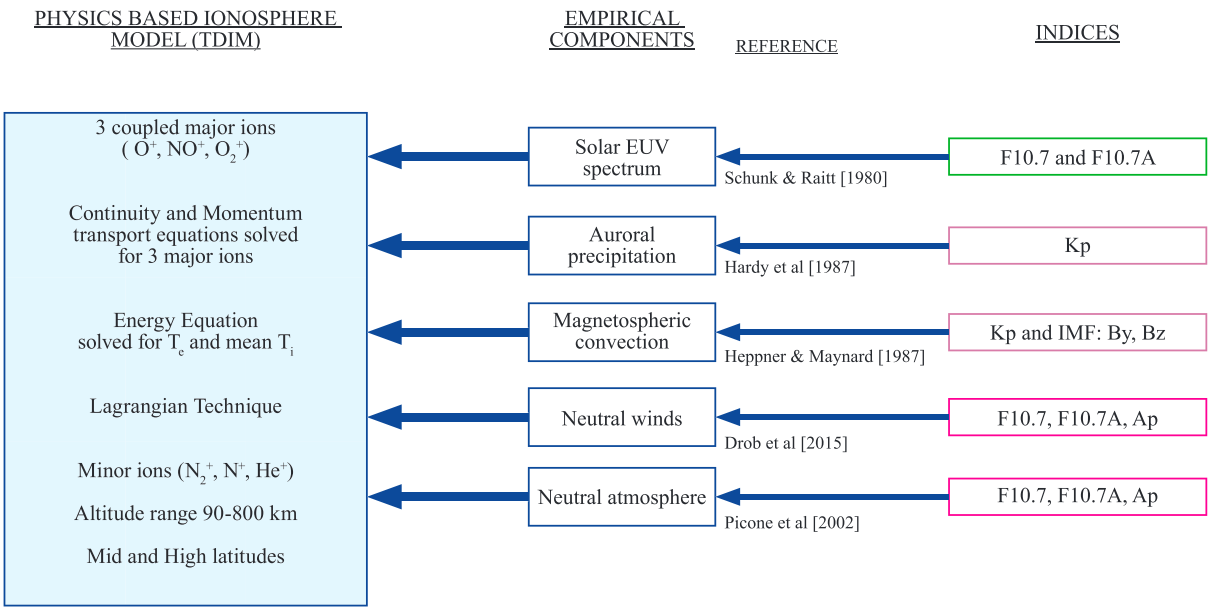

Figure 3. Block diagram describing how the Time Dependent Ionospheric Model is configured (left, blue block), driven by indices (right blocks) that select empirical model conditions (middle blocks). Each of the five empirical models has their associated citations.

ionogram analyses suggest that the difference between these locations of F2 peak (h_mF_2) could be tens of kilometers (Jackson, 1969). Similarly, and especially during storm conditions, our analysis would increase this uncertainty in the accuracy of the lowest height. For the purpose of this initial ISIS-II and TDIM study, observation, and modeling of the polar ionosphere's topside, we will emphasize the region above the F2 peak up to 800 km, the upper boundary of the TDIM model. An interesting difference between the lowest heights during the storm will be examined in the discussion section.

3. Ionospheric Model

The Utah State University TDIM is primarily an *F* region, 3-D, multi-ion model of the high- and middle-latitude ionosphere (Schunk, 1988; Sojka, 1989). The topside is dominated by O^+ at these latitudes, and TDIM has upper boundary conditions set at an altitude of 800 km. TDIM is a first-principles model that numerically solves continuity, momentum, and energy equations. Sojka et al. (2013, and references therein) provide descriptions of the model usage and development.

For this particular set of simulations, the TDIM was configured as shown in Figure 3. To replicate the conditions for the study period, the following indices were used: Kp (ap), F10.7, and F10.7A. Each had its own temporal resolution as shown in Figure 1. For the magnetospheric convection, the Heppner and Maynard (1987) model was used and the A pattern was adopted to represent the dependence upon interplanetary magnetic field conditions. The convection electric field strength was driven by the Kp dynamics shown in Figure 1, middle row. This geomagnetic index also determined the dynamics of the auroral electron precipitation that was empirically represented by the Hardy et al. (1987) model. The neutral atmosphere is empirically represented by the NRLMSIS model (Picone et al., 2002) and the neutral winds model (Drob et al., 2015). Both these models use the solar radio flux indices F10.7 and F10.7A (see Figure 1, lower row) along with the ap geomagnetic index. The ap index was derived from the Kp index shown in the middle row of Figure 1. The solar EUV ionization model is described by Schunk and Raitt (1980).

The emphasis of this study is the modeling of the topside ionosphere and a comparison of the simulations with the observed ISIS-II topside ionograms during two geomagnetic storms. At this time, no observations have been used to constrain the model topside boundary for either number or energy flux. Therefore, for this initial study these are set to default flux conditions specified by Schunk (1988). The topside boundary is located at an altitude of 800 km.

4. Topside Ionosphere Comparisons

4.1. Model Simulations

The TDIM was run in storm mode over a period of more than 24 hr, leading up to the locations and times when ISIS-II made ionogram observations. The geomagnetic and solar indices shown in Figure 1 provided the storm history. The TDIM solves the differential equations using a Lagrangian method. Hence, single TDIM simulations of a plasma flux tube are followed to the location and time where an ISIS-II ionogram was observed. The limitation in accuracy of this approach is less than a few degrees in latitude, half an hour in local time and five minutes in time. The accuracy in the past history of the TDIM calculation depends on how well the Figure 1 indices represent the storm evolution or how well the indices are able to reproduce the necessary atmospheric and magnetospheric drivers specified in Figure 3. These modeling procedures create a TDIM EDP for every ISIS-II EDP shown in Figures 2b and 2d, a total of 59 electron density topside profiles.

4.1.1. STORM1 Topside Ionosphere

The TDIM simulations extend from 90 to 800 km in altitude, while the ISIS-II topside analysis extends downward from about 1,400 km to a lowest height. TDIM has a variable output altitude step size, ranging from 4 km at low altitudes to 100 above 600 km, while the topside ionogram inversion uses a 1-km step from 1,400 km downward. In order to establish a working definition of topside, the following procedure is adopted.

1. The TDIM O^+ peak height is the lowest altitude.
2. The TDIM upper boundary of 800 km is the highest altitude.
3. ISIS-II EDP densities are taken at altitudes corresponding to a TDIM density altitude location.

The topside EDP comparisons for the two ISIS-II passes for STORM1 are shown in the top two panels of Figure 4. The geomagnetically quiet pass is shown in the left panel. This quiet pass had 11 EDPs, and these are shown as lines, while the corresponding 11 TDIM EDPs are shown as unconnected diamonds. These topside EDPs range upward in altitude from about 300 km. Morphologically, the 11 ISIS-II EDPs have similar shapes and span a density range of a factor of two at any specific altitude, and the corresponding TDIM EDPs have a much wider density range, about a factor of 4. However, the independent sets of EDPs share the same electron density envelope. It could be argued that the ISIS-II are somewhat steeper, that is, have a larger scale height than the TDIM values. This will be analyzed further in a later subsection. Below 400 km, about half of the TDIM electron densities are up to a factor of 2 larger than any of the ISIS-II densities. The top right panel in Figure 4 presents the STORM1 21 EDPs during the storm pass. Overall, the trend is for the TDIM topside to be somewhat more dense than the ISIS-II EDPs, especially at the altitudes below 400 km where this difference could be more than a factor of 2. Compared to the quiet pass, top left, the electron densities are overall systematically lower during the storm. An interesting aspect of this comparison is that if only information about the peak, N_mF_2 was available, it would be reasonable to conclude that the model was overestimating the density by more than a factor of 2, but as the topside data are available quite a different conclusion is reached about the model-observation comparison.

4.1.2. STORM2 Topside Ionosphere

The quiet pass topside EDP comparison associated with STORM2 is shown in the bottom left panel in Figure 4. A total of 13 EDPs for ISIS-II is plotted as lines. These are very tightly packed and are consistent with the presentation shown in Figure 2d, left panel. The 13 TDIM profiles are shown as unconnected diamonds and are also tightly distributed very close to those of ISIS-II. The STORM2 storm pass occurred at a time when the Kp was close to 8+ and the Dst approached −200 nT, a significantly stronger geomagnetic storm than STORM1. The bottom right panel shows the 14 EDPs from ISIS-II as lines and those of the TDIM as unconnected symbols. The model and observation densities are significantly different; all ISIS-II densities were lower than the lowest TDIM density. However, many of the scale heights are similar. The lowest altitude set by the TDIM O^+ peak height has almost reached 500 km. The spread in density values for both the model and ISIS-II values is well over a factor of 2. In the next subsection, a detailed analysis of the topside electron density comparisons shown in Figure 4 is given.

4.2. Statistical Analysis of Topside Comparison

A topside ionogram comparison for each pair of profiles was carried out and is presented in Figure 5 for STORM1, upper panel, and STORM2, lower panel. We calculated a percentage difference (ISIS-II EDP-TDIM

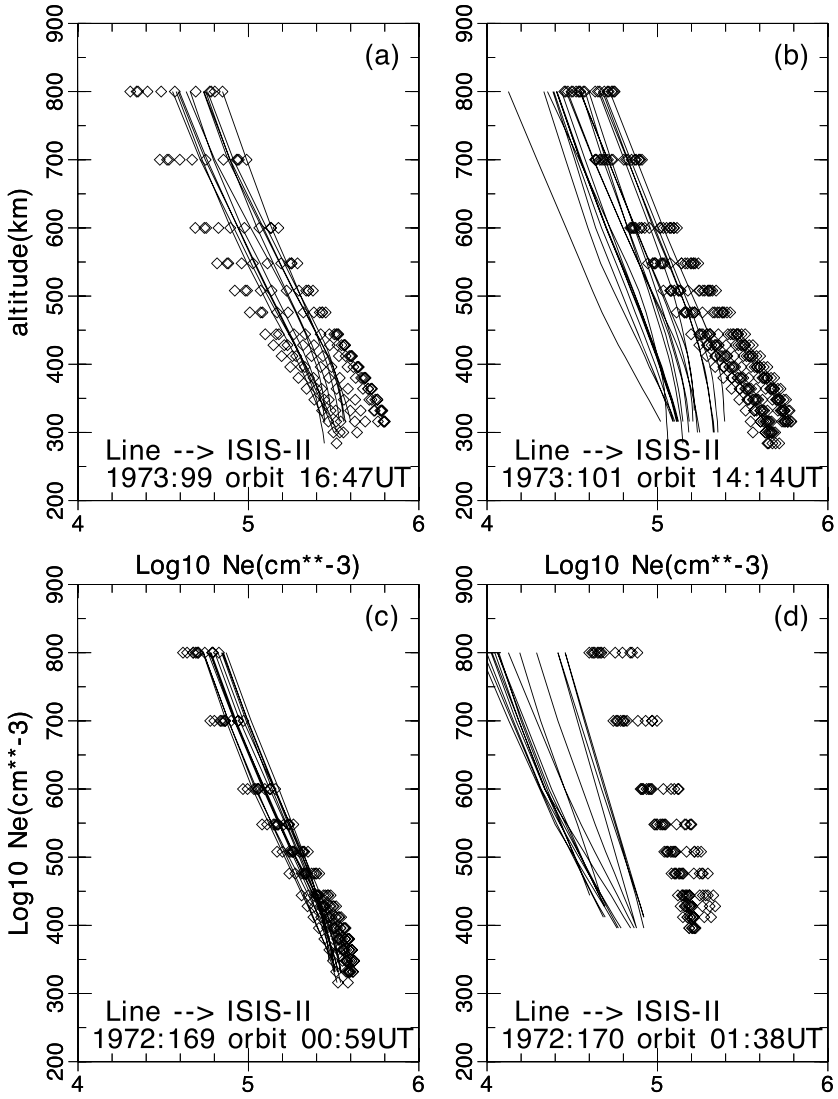

Figure 4. Topside EDP comparison between ISIS-II (lines) and TDIM simulations (diamond symbols). Each panel contains all the ISIS-II inversions of ionograms to EDP for a specific orbit pass. A TDIM simulation corresponding to each ISIS-II EDP is shown. The orbit ephemeris information is included in each panel. ISIS = International Satellites for Ionospheric Studies; EDP = electron density profile; TDIM = Time Dependent Ionospheric Model.

EDP)*100/(ISIS-II EDP) at each altitude. This is the method of analysis used by Nishida (1967) and Sato and Chan (1969). Then an average percentage difference for the topside EDP was calculated from these individual percentages. Figure 5, top panel, shows the result of this EDP average percentage difference for each of the 11 ISIS-II ionograms shown in Figure 4, top left panel. The first three averages, midnight sector show a positive average percentage difference, ranging from 9.7% to 27.3%. All the other differences are negative, indicating that ISIS-II topside densities are smaller by a factor ranging from −9.2% to −79.1%. Figure 4, top left panel, would suggest that these negative differences are mainly due to the lower altitude difference. Figure 5, top panel diamond line, repeats this analysis for the STORM1 storm pass, 21 ionograms. In this case, all the average percentage differences are negative. The profiles for the second half of the pass across the polar region into the dayside prenoon sector all have average percentage differences of magnitude greater than 100% up to 442.6% which are negative, indicating that the ISIS-II densities are over a factor of 2 lower than those of the TDIM. As with the quiet pass for this storm, Figure 4, top right panel, suggests that these large differences are mainly caused by even larger differences at the lowest altitudes.

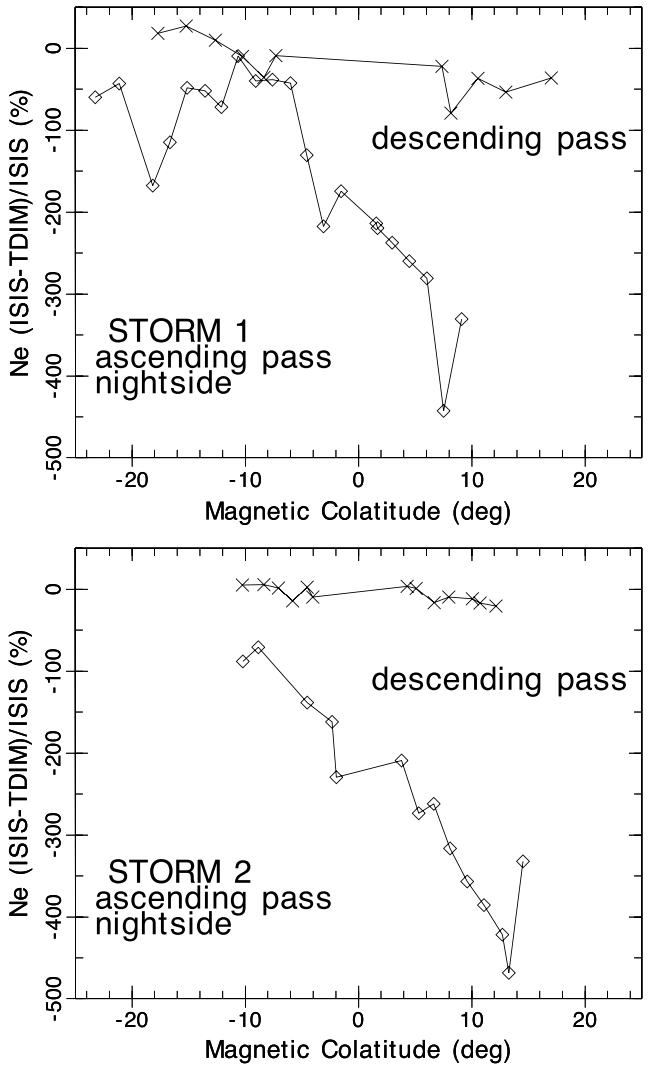

Figure 5. Top panel contrasts topside Ne percentage difference (defined in text) for STORM1 quiet pass, line with x symbols, and disturbed pass, line with diamonds. Bottom panel repeat percent difference for STORM2. The negative colatitudes correspond to International Satellites for Ionospheric Studies-II moving poleward in latitude on the nightside and then equatorward, positive colatitudes.

The STORM2 quiet pass, Figure 5, bottom panel x line, and storm pass, Figure 5, bottom panel diamond line, are dramatically different. In the quiet pass, the 13 profiles of ISIS-II and TDIM are to all intents equivalent. The average percentage difference ranges from −20.5% to 5.5%. These 13 topside profiles range in location from an evening sector location of 79.7° magnetic latitude, 22.6 hr magnetic local time across the polar cap to a morning sector location of 77.9°magnetic latitude, 8.0 hr magnetic local time. The lack of overall differences between the profiles, Figure 4, left bottom panel, is readily attributable to the quiet geomagnetic conditions and full sunlit, polar cap summer solstice conditions. Once the storm occurs, this situation changes dramatically as indicated by Figure 5, bottom panel diamond line. In all cases, the ISIS-II densities are lower and all average percentage difference are much more negative, ranging from −70.9% to −468.5%. In this pass, the large differences are not a result of the lower altitudes being excessively different; see Figure 4, bottom right panel. Indeed, it may be argued that the higher topside densities show a somewhat larger difference.

4.3. Topside Scale Heights

The prior two subsections involved comparisons of altitude EDPs between the ISIS-II observations and TDIM simulations. The shape of these profiles is a function of ion composition, ion temperature, and electron temperature under diffusive equilibrium conditions. However, as Kp increases, other forms of outflow and heating would lead to modifications in the profile shape. The altitude distribution of the plasma scale height is a representation of the diffusive/nondiffusive physical mechanisms. We follow the method used by Watt (1965) for extracting a plasma scale height parameter from the topside EDP, namely, $Hp = -\mathrm{Ne}/(d\mathrm{Ne}/dz)$ where Ne is the density at height z. Hence, the 59 EDPs shown in Figure 4 were converted to Hp profiles. Note that if the composition is dominated by one ion, that is, O^+, and both T_e and T_i are constant, the Hp profile would be constant with altitude under diffusive equilibrium conditions.

4.3.1. STORM1

The ISIS-II Hp profiles are shown in the left panels of Figure 6 with the quiet pass in the bottom panel and the storm pass in the upper panel. Between 500 and 800 km, Hp increases smoothly from 220 to 300 km for the quiet pass. However, below this region, Hp increases rapidly as altitude decreases. This latter effect is associated with the approach to the F2 layer peak at h_mF_2. During the storm pass, top left panel, above 500 km, the scale height is more constant at 300 km ± 50 km, while below this altitude, it is either increasing rapidly or in some cases decreasing slightly.

The right column of Figure 6 presents the Hp profiles for the corresponding TDIM simulations. These are less spread but show similar profile morphology to that found in the ISIS-II profiles. The quiet pass TDIM Hp, bottom right panel, from 500 to 800 km has Hp increasing from 150 to 300 km. Below about 400 km, Hp increases. Both of these trends are similar to the quiet ISIS-II profile. During the storm pass, the TDIM scale heights are lower by as much as 100 at 500 km compared to the corresponding ISIS-II profiles. The simulated storm scale heights then increase rapidly with increasing altitude below about 400 km, again a different morphology from the ISIS-II storm profiles. The increases in the TDIM storm scale heights in this region are at much lower altitudes than those of the ISIS-II storm profiles.

4.3.2. STORM2

The quiet pass ISIS-II Hp and TDIM Hp profiles, lower panels of Figure 7, are very similar. This is to be expected based on Figure 4, bottom left panel. They also compare favorably with the quiet day results for STORM1. However, the storm pass of STORM2 upper panels, Figure 7, is very different from the quiet pass results.

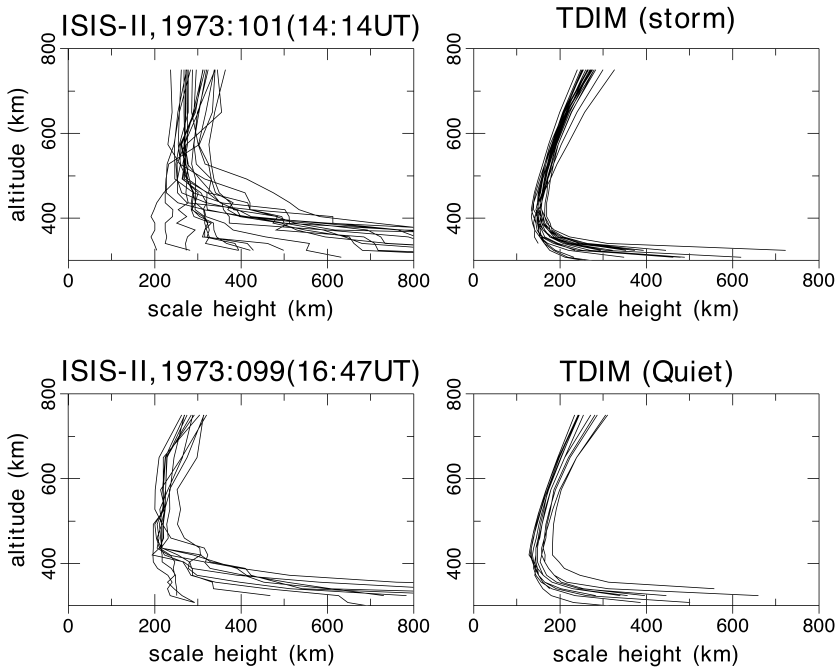

Figure 6. Computed scale heights for ISIS-II electron density profile (left panels) and for TDIM simulations (right panels) for the 1973, day 99 quiet pass (lower panels) and for the 1973, day 101 storm pass (upper panels). ISIS = International Satellites for Ionospheric Studies; TDIM = Time Dependent Ionospheric Model.

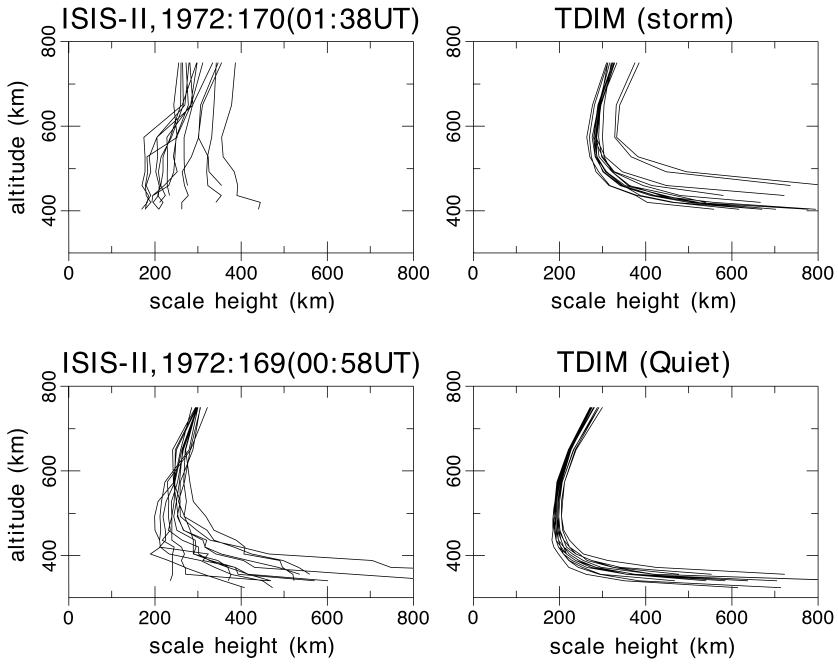

Figure 7. Computed scale heights for ISIS-II electron density profile (left panels) and for TDIM simulations (right panels) for the 1972, day 169 quiet pass (lower panels) and for the 1972, day 170 storm pass (upper panels). ISIS = International Satellites for Ionospheric Studies; TDIM = Time Dependent Ionospheric Model.

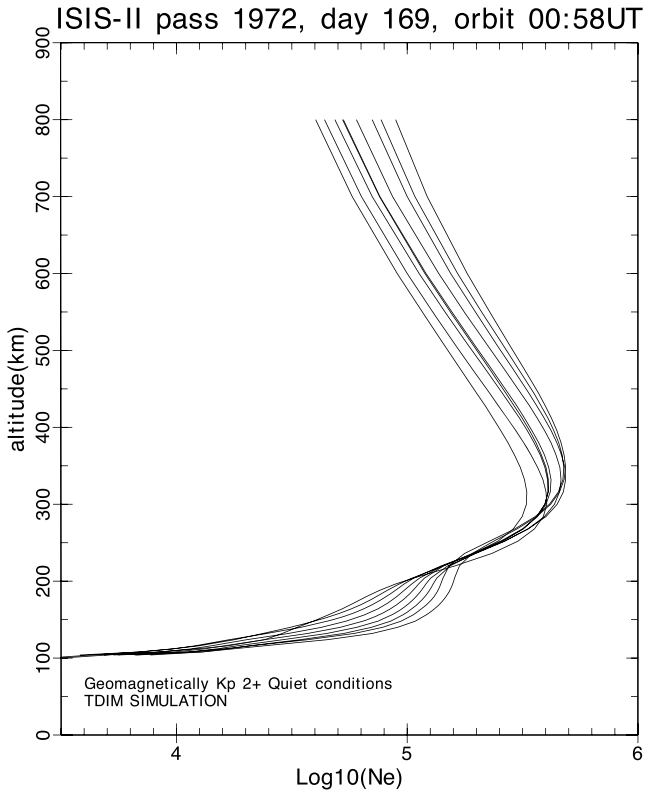

Figure 8. Time Dependent Ionospheric Model simulated Ne altitude profiles, corresponding to all the ISIS-II ionograms obtained on day 169, 1972, shown in Figure 4, bottom left panel. ISIS = International Satellites for Ionospheric Studies.

The TDIM simulations, top right panel, Figure 7, show that the entire Hp shape has been shifted upward in altitude by over 150 km compared to the quiet case. Also, the Hp values have increased over the quiet pass by over 100 km (50%) at altitudes around 600 km. Although the ISIS-II storm pass shows almost no increase in Hp at upper altitudes, the lower altitudes show a very large range of Hp values, ranging from under 200 to over 400 km. These Hp profiles show only a slight increase in Hp with altitude. The major difference between TDIM and ISIS-II profiles is that the lowest altitude defined by the O^+ peak altitude in the TDIM simulation can be much higher than the actual lowest altitude of the ISIS-II observation. The similarity lies in the highest altitudes where both model and observations have Hp ranging from 300 to 400 km, while for the quiet pass, the range of Hp is smaller, around *Hp* = 300 km.

5. Discussion

Watt (1965, 1966) carried out topside scale height analysis of Alouette-1 topside ionograms. He showed that poleward of 62° dip latitude, the transition height between O^+ and the light ions (H^+ and He^+) was above 900 km (see Figure 9 of Watt, 1965). This result is the basis for our assumption throughout our topside high-latitude study that O^+ is the dominant ion up to 800 km. Watt (1965, Figure 2) describes the higher dip latitudes, 60–69°as having Hp ranging from 150 to 200 km at 400-km altitude, increasing to 250–350 km at 800-km altitude. Our findings during quiet time conditions are consistent with these results. However, Watt (1966) suggests that there is no Kp dependence in the dayside topside ionosphere although a dependence is found in the nightside. This suggestion is quite different from our findings as seen in Figures 4–7 where both storm passes suggest that as Kp increases, the topside dayside exhibits a strong response by decreasing the electron density and increasing the scale height. It is important to note, however, that the Watt studies only extended from low to midlatitudes up to about 70°dip latitude, whereas our four passes downlinked to Resolute Bay, Canada, only receive topside ionograms observed poleward of 70° magnetic latitude. Similarly, the Watt studies only show scale heights at altitudes well above the F2 layer peak. But our results include those scale heights calculated from the O^+ peak upward. This location is based on the TDIM simulations upward of the O^+ peak density. In the region immediately above this peak, the scale heights are large, decreasing to a minimum. At this altitude and above, our scale heights can be compared with those of Watt (1965, 1966). Including this lower region provides a more structured representation of the *upper* ionosphere. In turn, it provides additional information when making the observation-model comparison. The case in point shows that the first three pass comparisons, STORM1 quiet and storm and the STORM2 quiet, all exhibit almost the same ISIS-II and TDIM Hp morphologies. However, the STORM2 storm pass does not. In this case, the TDIM Hp starts at a higher altitude, 450 km, with the large Hp values associated with the O^+ peak. Moreover, the ISIS-II Hp shows no indication of these large Hp values, suggesting that the ionospheric peak must be well below this altitude.

Even with only four passes, the study so far highlights interesting behavior exhibited during storm time where the model and observations during the Kp 8+ pass appear inconsistent with each other. The storm simulations appear to place the *F* layer much higher than the observations and higher than the quiet time model or observations. While the comparisons in Figure 2b and 2d suggest that during the storm, the lowest altitude near the ionospheric peak is lower than on the quiet prestorm pass. A resolution to this contradiction may lie in the response of ionospheric composition changes in response to both heating and $\mathbf{E} \times \mathbf{B}$ vertical transport enhanced during storms, especially during severe geomagnetic storms such as STORM2. Figure 8 shows all the TDIM simulated EDPs used in this study, ranging from 100 to 800 km for the STORM2 quiet pass. For these EDPs, the F2 layer peak, h_mF_2 lies between 290 and 340 km. Below the peak lies a weak F1 centered at about 150 km. Figure 9 shows the STORM2 storm pass EDPs. These are markedly different from the quiet pass but are consistent with the Kp 8+ conditions as follows:

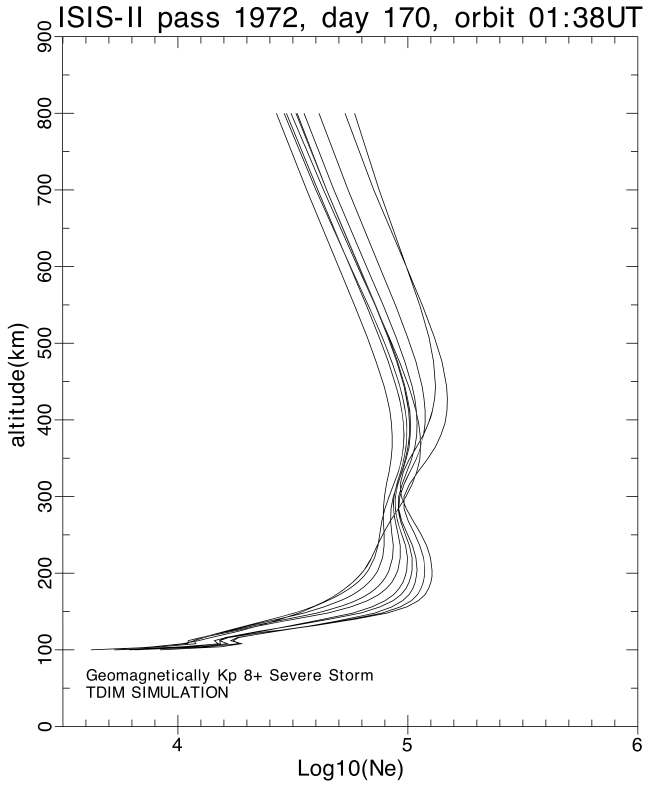

Figure 9. TDIM simulated Ne altitude profiles, corresponding to all the ISIS-II ionograms obtained on day 170, 1972, shown in Figure 4, bottom right panel. ISIS = International Satellites for Ionospheric Studies; TDIM = Time Dependent Ionospheric Model.

1. The heating has led to enhanced plasma temperatures.
2. In response, the O^+ is being rapidly converted to NO^+.
3. O^+ is a dominant F2 ion whereas NO^+ is the dominant F1 ion.
4. As a result, F1 is increasing in density while F2 is decreasing. The TDIM simulations show that for some of the profiles, the F1 peak density exceeds the F2.
5. In ionogram scaling, this is referred to as the ionospheric G condition in which the lower layer is dominant and the F2 layer is not observed from a ground-based ionosonde.

This G condition seen from the topside will, however, enable the topside sounder to see below the F2 layer down to the peak of the F1 layer. In Figure 9, the difference in height between the F2 and F1 peaks ranges from 100 to over 200 km. The implication of this for the STORM2 quiet storm pass comparison is that, if indeed, this G condition was present, then the lowest EDP altitudes should occur for the storm case, as is seen. This would also partially explain the scale height difference between the observations and the model for the STORM2 storm pass. The adopted definition of topside was that the altitude above the modeled O^+ peak was in the topside. But as Figure 9 shows, this peak need not, in fact, be the ionospheric density peak. A further complication is that the dayside ionospheric O^+ peak has been raised by very strong poleward $\mathbf{E} \times \mathbf{B}$ flows that raise the layer. During the actual event, the knowledge necessary to determine how strong this uplift should be is unavailable. The Kp 8+ condition is probably driving the empirical Heppner and Maynard (1987) cross polar cap potential to much larger values than was realized. The model evidence for the plasma heating is noted by comparing the quiet topside scale heights with those of the storm, that is, by comparing the simulated Ne profiles of Figures 8 and 9. These figures indicate that the storm scale heights are larger indicating a hotter plasma temperature. An indication of this difference is also found when comparing these two passes from ISIS-II during STORM2, Figure 7, left panels. Our storm modeling analysis fails to capture the marked factor of 4 and larger dayside decrease. This we attribute to the difficulty of driving the TDIM with a large topside outflow. Otherwise, the physics described is consistent with earlier storm simulations of the TDIM (Sojka et al., 1981, 1982). Norton (1969) described exactly the same scenario for storm response, seen in both topside and ground-based ionograms.

His Figure 1, showing storm and quiet ionospheric profiles at St. John's, Newfoundland on 18 April 1965, can be readily compared with the TDIM simulations in our Figures 8 and 9. Norton (1969) attributes the storm effect to the enhanced loss rate for O^+, which is our item 2, listed above.

Benson et al. (2016) studied 10 large geomagnetic storms, using topside sounder EDPs from several of the ISIS program satellites. They suggested that some of the large storm-induced topside Ne profile changes observed at high latitudes could be related to changes in specific solar wind parameters. An extension of our present study will be to carry out ionospheric simulations for these cases, especially since well-defined interplanetary magnetic field information is available. In their study, Benson et al. (2016) used a different approach than that used in the present study. Rather than comparing two polar cap satellite passes, one before and one during a storm, they compared profiles that were representatives of groups of profiles collected in the same small region of space for a given storm over several days before, during, and after the storm. Both large increases and decreases were observed depending on conditions.

In their introduction, they give a detailed literature review with examples of both storm negative and storm positive responses that have been observed in the topside ionogram data. Our study adds two sets of polar cap passes from two storms. Significantly, more storm EDP passes are needed to create meaningful test conditions for modeling studies.

This study demonstrates deficiencies in modeling the ionospheric response to a severe Kp 8+ geomagnetic storm. In particular, an ionospheric model with an upper boundary of 800 km was most likely inadequate in

representing the outflow of ionospheric conditions during the storm. Indeed, polar wind models are probably needed to capture the M-I outflow physics. Although not shown, the TDIM was run with somewhat aggressive outflow boundary conditions and was still unable to capture the factor of 4 reduction in EDP density that was observed. This suggests that there are additional reasons for the poor model-data comparison. In both storm comparisons the modeled F1 region densities were too high during storm conditions, which may keep the topside too dense regardless of the ion outflow rates. The dense F1 region might result if the Mass Spectometer and Incoherent Scatter (MSIS) constituent specification or the reaction rates used for the ion chemistry are deficient during the storm conditions. Additionally, significant suprathermal electrons at these lower altitudes may enhance the extraction of plasma from these lowest altitudes.

6. Summary

We have carried out a topside ionosphere comparison of the model simulations from the TDIM and observations made by the ISIS-II satellite's topside sounder. Our studies focused on a moderate, Kp 5−, and a severe Kp 8+, geomagnetic storm with data downlinked to the polar cap ground station at Resolute Bay, Canada. The main findings of the study are the following:

1. During prestorm conditions, the model to observation agreement is very good.
2. During the Kp 5− STORM1 pass, the trend shows that the observed EDP density is lower than that of prestorm conditions. However, the model densities do not follow these data.
3. During the Kp 8+ STORM2 storm pass, the model was unable to simulate a factor of 4 decrease in the EDPs of ISIS-II observations compared to their prestorm values.
4. The physical processes modeled during the storm imply that significant heating has led to an ionospheric G condition, which is consistent with the ISIS-II observations over the 14 ionograms of the STORM2 storm pass.

The major difficulty with the methodology of this study is that only one severe geomagnetic storm data set is available. To make progress in testing and validating topside ionospheric simulations, additional topside data sets are needed. This study makes the case that this model, TDIM, was unable to replicate the ionospheric response to a severe geomagnetic storm. With additional storm data sets the specific reasons for the failure would be open to investigation. This result has important implications since the TDIM has had over 30 years of very good bottomside and peak ionosphere agreement with observations. The use of observations made across the entire polar cap provides evidence of how large scale rather than local scale the storm response is. The satellite topside sounder generates these large-scale observations that in fact complements the high time resolution but relatively local observations made by the ISR technique.

Future work needs to focus on the acquisition of more topside passes. This requires further topside ionogram inversion so that entire passes are available. In parallel to this data retrieval, a study using polar wind models needs to be run, using the ISIS topside data as ground truth in comparisons similar to those we have made in this study.

Acknowledgments
This work was supported by NSF grant AGS-0962544 to Utah State University and by NASA awards NNH14CL84C and 80HQTR17C0023 to Space Environment Corporation. Data policy: ISIS-II 35-mm films were made available to SEC from the film archive of the Communications Research Centre, Ottawa, Canada. Reduced ionograms and inverted ionogram data are archived at NASA Space Physics Data Facility (SPDF), while ionospheric simulations have been archived at http://digitalcommons.usu.edu/all_datasets/43/. Data are archived at DigitalCommons @ USU and is available at https://doi.org.10.15142/T30926.

References

Benson, R. F. (1996). Ionospheric investigations using digital Alouette/ISIS topside ionograms. In J. M. Goodman (Ed.), *Proceedings of 1996 ionospheric effects symposium* (pp. 202–209). Alexandria, VA: National Technical Information Service.

Benson, R. F. (2010). Four decades of space-borne radio sounding. *Radio Science Bulletin*, *333*, 24–44.

Benson, R. F., & Bilitza, D. (2009). New satellite mission with old data: Rescuing a unique data set. *Radio Science*, *44*, RS0A04. https://doi.org/10.1029/2008RS004036

Benson, R. F., Fainberg, J., Osherovich, V. A., Truhlik, V., Wang, Y., Bilitza, D., & Fung, S. F. (2016). High-latitude topside ionospheric vertical electron density profile changes in response to large magnetic storms. *Radio Science*, *51*, 524–537. https://doi.org/10.1002/2015RS005882

Benson, R. F., Truhlik, V., Huang, X., Wang, Y., & Bilitza, D. (2012). Improving the automatic inversion of digital Alouette/ISIS ionogram-reflection traces into topside electron-density profiles. *Radio Science*, *47*, RS0L04. https://doi.org/10.1029/2011RS004963

Bilitza, D. (2009). Evaluation of the IRI-2007 model options for the topside electron density. *Advances in Space Research*, *44*(6), 701–706. https://doi.org/10.1016/j.asr.2009.04.036

Chan, K. L., & Colin, L. (1969). Global electron density distributions from topside soundings. *Proceedings of the IEEE*, *57*(6), 960–976. https://doi.org/10.1109/PROC.1969.7140

Daniels, F. (1971). *ISIS-II spacecraft, Communications Research Centre*. Ottawa, Canada: Department of Communications.

Dayharsh, T. I., & Farley, W. W. (1965). Electron density variations at 1000 kilometers. *Journal of Geophysical Research*, *70*(21), 5361–5368. https://doi.org/10.1029/JZ070i021p05361

Drob, D. P., Emmert, J. T., Meriwether, J. W., Makela, J. J., Doornbos, E., Conde, M., et al. (2015). An update to the horizontal wind model (HWM): The quiet time thermosphere. *Earth and Space Science*, *2*(7), 301–319. https://doi.org/10.1002/2014EA000089

Foster, J. C., Coster, A. J., Erickson, P. J., Holt, J. M., Lind, F. D., Rideout, W., et al. (2005). Multiradar observations of the polar tongue of ionization. *Journal of Geophysical Research*, *110*, A09S31. https://doi.org/10.1029/2004JA010928

Hardy, D. A., Gussenhoven, M. S., Raistrick, R., & McNeill, W. J. (1987). Statistical and functional representations of the pattern of auroral energy flux, number flux, and conductivity. *Journal of Geophysical Research*, *92*(A11), 12,275–12,294. https://doi.org/10.1029/JA092iA11p12275

Heppner, J. P., & Maynard, N. C. (1987). Empirical high-latitude electric field models. *Journal of Geophysical Research*, *92*(A5), 4467–4489. https://doi.org/10.1029/JA092iA05p04467

Institute of Electrical and Electronics Engineers (1969). Special topside issue. *Proceedings of the IEEE*, *57*(6), 960–976. https://doi.org/10.1109/PROC.1969.7140

Jackson, J. E. (1969). Comparison between topside and ground-based soundings. *Proceedings of the IEEE*, *57*(6), 976–985. https://doi.org/10.1109/PROC.1969.7141

Jackson, J. E., Schmerling, E. R., & Whitteker, J. H. (1980). Mini-review on topside sounding. *IEEE Transactions on Antennas and Propagation*, *28*(2), 284–288. https://doi.org/10.1109/TAP.1980.1142318

Kitamura, N., Nishimura, Y., Chandler, M. O., Moore, T. E., Terada, N., Ono, T., et al. (2012). Storm-time electron density enhancement in the cleft ion fountain. *Journal of Geophysical Research*, *117*, A11212. https://doi.org/10.1029/2012JA017900

Kitamura, N., Nishimura, Y., Ono, T., Kumamoto, A., Shinbori, A., Lizima, M., et al. (2010). Temporal variations and spatial extent of the electron density enhancements in the polar magnetosphere during geomagnetic storms. *Journal of Geophysical Research*, *115*, A00J02. https://doi.org/10.1029/2009JA014499

Lockwood, M., & Titheridge, J. E. (1981). Ionospheric origin of magnetospheric O^+ ions. *Geophysical Research Letters*, *8*(4), 381–384. https://doi.org/10.1029/GL008i004p00381

Nishida, A. (1967). Average structure and storm-time change of the polar topside ionosphere at sunspot minimum. *Journal of Geophysical Research*, *72*(23), 6051–6061. https://doi.org/10.1029/JZ072i023p06051

Norton, R. B. (1969). The middle-latitude F region during some severe ionospheric storms. *Proceedings of IEEE*, *57*(6), 960–976. https://doi.org/10.1109/PROC.1969.7140

Ogawa, Y., Fujii, R., Buchert, S. C., Nozama, S., & Ohtani, S. (2003). Simultaneous EISCAT Svalbard radar and DMSP observations of ion upflow in the dayside polar ionosphere. *Journal of Geophysical Research*, *108*(A3), 1101. https://doi.org/10.1029/2002JA009590

Osherovich, V. A., Benson, R. F., Fainberg, J., Green, J. L., Garcia, L., Boarsden, S., et al. (2007). Enhanced high-altitude polar-cap plasma and magnetic-field values in response to the interplanetary magnetic cloud that caused the great storm of 31 March 2001: A case study for a new magnetospheric index. *Journal of Geophysical Research*, *112*, A06247. https://doi.org/10.1029/2006JA012105

Picone, J. M., Hedin, A. E., Drob, D. P., & Aiken, A. C. (2002). NRLMSISE-00 empirical model of the atmosphere: Statistical comparisons and scientific issues. *Journal of Geophysical Research*, *107*(A12), 1468. https://doi.org/10.1029/2002JA009430

Reinisch, B. W., Nsumei, P., Huang, X., & Bilitza, D. K. (2007). Modeling the F2 topside and plasmasphere for IRI using IMAGE/RPI and ISIS data. *Advances in Space Research*, *39*(5), 731–738. https://doi.org/10.1016/j.asr.2006.05.032

Rice, D. D., Eccles, J. V., Sojka, J. J., James, H. G., & Benson, R. F. (2015). Expanding the topside sounder digital data collection. Proceedings of IES-2015. Retrieved from http://ies2015.bc.edu/wp-content/uploads/2015/08/IES2015-Proceedings.pdf

Rice, D. D., Sojka, J. J., Eccles, J. V., James, H. G., Torre, C., & Benson, R. F. (2017). Ensemble inversion method for ISIS II topside ionograms, Proceedings of IES-2017. Retrieved from https://ies2017.bc.edu/wp-content/uploads/2017/05/5B2-RiceIES-Topside_d2-Paper.pdf

Sato, T., & Chan, K. L. (1969). Storm-time variations of the electron concentration in the polar topside ionosphere. *Journal of Geophysical Research*, *74*(9), 2208–2216. https://doi.org/10.1029/JA074i009p02208

Sato, T., & Colin, L. (1969). Morphology of electron concentration enhancement at a height of 1000 kilometers at polar latitudes. *Journal of Geophysical Research*, *74*(9), 2193–2207. https://doi.org/10.1029/JA074i009p02193

Schunk, R. W. (1988). A mathematical model of the middle and high-latitude ionosphere. *Pure and Applied Geophysics*, *127*(2-3), 255–303. https://doi.org/10.1007/BF00879813

Schunk, R. W., & Raitt, W. J. (1980). Atomic nitrogen and oxygen ions in the daytime high-latitude F region. *Journal of Geophysical Research*, *85*(A3), 1255–1272. https://doi.org/10.1029/JA085iA03p01255

Sojka, J. J. (1989). Global scale, physical models of the F-region ionosphere. *Reviews of Geophysics*, *27*(3), 371–403. https://doi.org/10.1029/RG027i00371

Sojka, J. J., Jensen, J., David, M., Schunk, R. W., Woods, T., & Eparvier, F. (2013). Modeling the ionospheric E and F1 regions: Using SDO-EVE observations as the solar irradiance driver. *Journal Geophysical Research: Space Physics*, *118*, 5379–5391. https://doi.org/10.1002/jgra.50480

Sojka, J. J., Raitt, W. J., & Schunk, R. W. (1981). Plasma density features associated with strong convection in the winter high-latitude F region. *Journal of Geophysical Research*, *86*(A8), 6908–6916. https://doi.org/10.1029/JA086iA08p06908

Sojka, J. J., Schunk, R. W., & Raitt, W. J. (1982). Seasonal variations of the high-latitude F region for strong convection. *Journal of Geophysical Research*, *87*(A1), 187–198. https://doi.org/10.1029/JA087iA01p00187

Titheridge, J. E., & Andrews, M. K. (1967). Changes in the topside ionosphere during a large magnetic storm. *Planetary and Space Science*, *15*(7), 1157–1167. https://doi.org/10.1016/0032-0633(67)90100-6

Tu, J.-N., Dhar, M., Song, P., Reinisch, B. W., Green, J. L., Benson, R. F., & Coster, A. J. (2007). Extreme polar cap density enhancements along magnetic field lines during an intense geomagnetic storm. *Journal of Geophysical Research*, *112*, A05201. https://doi.org/10.1029/2006JA012034

Wahlund, J. E., Opgenoorth, H. J., Haggstrom, I., Winser, K. J., & Jones, G. O. L. (1992). EISCAT observations of topside ionospheric ion outflows during auroral activity: Revisited. *Journal of Geophysical Research*, *97*(A3), 3019–3037. https://doi.org/10.1029/91JA02438

Warren, E. S. (1969). The topside ionosphere during geomagnetic storms. *Proceedings of the IEEE*, *57*(6), 960–976. https://doi.org/10.1109/PROC.1969.7140

Watt, T. M. (1965). Ion distribution and temperature in the topside ionosphere obtained from the Alouette satellite. *Journal of Geophysical Research*, *70*(23), 5849–5859. https://doi.org/10.1029/JZ070i023p05849

Watt, T. M. (1966). Correlation of plasma scale height with Kp in the topside ionosphere. *Journal of Geophysical Research*, *71*(13), 3131–3140. https://doi.org/10.1029/JZ071i013p03131

Willmore, A. P. (1965). Geophysical and solar activity variations in the electron temperature of the upper F region. *Proceedings Royal Society (London), Series A*, *286*(1407), 537–558. https://doi.org/10.1098/rspa.1965.0163

Yuan, Z.-G., Deng, X.-H., & Wang, J.-F. (2008). DMSP/GPS observations of intense ion upflow in the midnight polar ionosphere associated with the SED plume during a super geomagnetic storm. *Geophysical Research Letters*, *35*, L19110. https://doi.org/10.1029/2008GL035462

Zeng, W., & Horwitz, J. L. (2007). Formula representation of auroral ionospheric O^+ outflows based on systematic simulations with effects of soft electron precipitation and transverse ion heating. *Geophysical Research Letters*, *34*, L06103. https://doi.org/10.1029/2006GL028632

Zeng, W., & Horwitz, J. L. (2008). Storm enhances densities (SED) as possible sources for Cleft Ion Fountain dayside ionospheric outflow. *Geophysical Research Letters*, *35*, L04103. https://doi.org/10.1029/2007GL032511

Zou, S., Ridley, A., Jia, X., Boyd, E., Nicolls, M., Coster, A., et al. (2017). PFISR observation of intense ion upflow fluxes associated with an SED during the 1 June 2013 geomagnetic storm. *Journal Geophysical Research: Space Physics*, *122*, 2589–2604. https://doi.org/10.1002/2016JA023697